Acta Crystallographica Section D
Biological Crystallography
ISSN 0907-4449

A suite of Switch I and Switch II mutant structures from the G-protein domain of FeoB

Miriam-Rose Ash,[a] Megan J. Maher,[a,b] J. Mitchell Guss[a] and Mika Jormakka[b]*

[a]School of Molecular Bioscience, University of Sydney, NSW 2006, Australia, and [b]Structural Biology Program, Centenary Institute, Sydney, NSW 2042, Australia

Correspondence e-mail: m.jormakka@centenary.org.au

Received 10 August 2011
Accepted 26 September 2011

PDB References: NFeoB, T35A mutant, GDP^{N} complex, 3b1y; T35S mutant, apo, 3b1z; E67A mutant, mGMPPNP complex, 3b1v; E67A mutant, GDP complex, 3b1w; E66A mutant, GMPPNP complex, 3b1x.

The acquisition of ferrous iron in prokaryotes is achieved by the G-protein-coupled membrane protein FeoB. This protein possesses a large C-terminal membrane-spanning domain preceded by two soluble cytoplasmic domains that are together termed 'NFeoB'. The first of these soluble domains is a GTPase domain (G-domain), which is then followed by an entirely α-helical domain. GTP hydrolysis by the G-domain is essential for iron uptake by FeoB, and various NFeoB mutant proteins from *Streptococcus thermophilus* have been constructed. These mutations investigate the role of conserved amino acids from the protein's critical Switch regions. Five crystal structures of these mutant proteins have been determined. The structures of E66A and E67A mutant proteins were solved in complex with nonhydrolyzable GTP analogues, the structures of T35A and E67A mutant proteins were solved in complex with GDP and finally the structure of the T35S mutant was crystallized without bound nucleotide. As an ensemble, the structures illustrate how small nucleotide-dependent rearrangements at the active site are converted into large rigid-body reorientations of the helical domain in response to GTP binding and hydrolysis. This provides the first evidence of nucleotide-dependent helical domain movement in NFeoB proteins, suggesting a mechanism by which the G-protein domain could structurally communicate with the membrane domain and mediate iron uptake.

1. Introduction

The integral membrane protein FeoB is a ferrous iron transporter in prokaryotes, and FeoB-mediated iron acquisition is essential for the virulence of many human pathogenic bacteria that thrive in anaerobic or acidic environments (Dashper *et al.*, 2005; He *et al.*, 2006; Naikare *et al.*, 2006; Robey & Cianciotto, 2002; Velayudhan *et al.*, 2000). FeoB is a three-domain protein consisting of a GTPase domain (G-domain) at its N-terminus (Marlovits *et al.*, 2002), followed by another globular cytoplasmic domain (the 'helical domain'), which is then linked to a C-terminal membrane-spanning domain. Together, the soluble G-domain and helical domain have been termed 'NFeoB' (Marlovits *et al.*, 2002) and the structure and nucleotide-binding properties of this ~30 kDa construct have been described for various organisms (Guilfoyle *et al.*, 2009; Ash *et al.*, 2010; Hung *et al.*, 2010; Petermann *et al.*, 2010; Hattori *et al.*, 2009). The G-domain was found to adopt a Ras-like G-protein fold, with the five-helix helical domain packed against it.

Table 1
Crystallization conditions for mutant NFeoBSt proteins.

	Protein/nucleotide mixture	Crystallization condition
GDP^{N}–T35A	5 mg ml^{-1} T35A, 10 m*M* $MgCl_2$, 0.8 m*M* GMPPNP	0.1 *M* MIB buffer pH 6.0, 25% PEG 1500
Apo-T35S	6.5 mg ml^{-1} T35S, 10 m*M* $MgCl_2$, 0.8 m*M* GMPPNP	0.1 *M* HEPES pH 7.5, 2% PEG 400, 2 *M* $(NH_4)_2SO_4$
mGMPPNP–E67A	7 mg ml^{-1} E67A, 10 m*M* $MgCl_2$, 0.5 m*M* mGMPPNP	0.2 *M* NaCl, 20% PEG 6000, 0.1 *M* HEPES pH 7.0
GDP–E67A	6 mg ml^{-1} E67A, 10 m*M* $MgCl_2$, 2 m*M* GDP	0.1 *M* ammonium acetate, 11% PEG 10 000, 0.1 *M* bis-tris pH 5.8†
GMPPNP–E66A	5 mg ml^{-1} E66A, 10 m*M* $MgCl_2$, 0.5 m*M* GMPPNP	0.1 *M* SPG buffer pH 6.0, 25% PEG 1500

† Optimized from an initial hit consisting of 0.1 *M* ammonium acetate, 0.1 *M* bis-tris pH 5.5, 17% PEG 10 000.

G-proteins are well characterized 'molecular switches', which utilize five conserved sequence motifs, G1–G5, for nucleotide recognition and hydrolysis. During the GTPase cycle, two regions of the protein, Switch I and Switch II, undergo structural rearrangements that transmit the 'on' or 'off' signal to downstream effectors. While GTP hydrolysis by the G-domain is essential for iron import by FeoB (Eng *et al.*, 2008; Hattori *et al.*, 2009; Marlovits *et al.*, 2002), various lines of evidence suggest that this domain does not act as a signalling molecule to other effector proteins but instead directly couples GTPase activity to iron import through the membrane domain (Eng *et al.*, 2008; Hantke, 2003). It follows that structural changes associated with the GTPase cycle must be communicated from the G-domain to the membrane domain, providing nucleotide-dependent gating of the ion-transport pathway as in other nucleotide-hydrolyzing transporters such as ABC proteins (Rees *et al.*, 2009) and P-type ATPases (Palmgren & Nissen, 2011). It has been hypothesized that this structural change could be communicated *via* the helical domain, which links the G-protein to the membrane domain (Hattori *et al.*, 2009; Petermann *et al.*, 2010). Indeed, mutations that disrupt the interface between the G-domain and helical domain not only influence the affinity of the domain for nucleotides, but also abrogate iron transport despite intact nucleotide hydrolysis (Eng *et al.*, 2008; Hattori *et al.*, 2009). However, no studies have yet been able to determine whether nucleotide-dependent movement of the helical domain does in fact occur.

Recently, we reported the structure of *Streptococcus thermophilus* NFeoB (NFeoBSt) bound to the transition-state analogue GDP–AlF_4^-, which gave insight into the mechanism by which the protein initiates the nucleotide-hydrolysis reaction (Ash *et al.*, 2011). In the same study, we generated a series of point mutations in NFeoBSt that explored the role of conserved amino acids in the Switch regions. Here, we present a series of five structures arising from four of these mutant proteins: T35A, T35S, E66A and E67A. Thr35 lies in the Switch I region and mediates GTP-induced Switch I movement by coordinating an essential Mg^{2+} ion that binds at the active site with GTP. In the T35A mutant protein the rate of GTP binding (Ash *et al.*, 2011) and the overall affinity for GTP (*Escherichia coli* NFeoB; Eng *et al.*, 2008) were both reduced. Furthermore, both T35S and T35A mutations abolished the GTPase activity of NFeoBSt (Ash *et al.*, 2011). Glu66 and Glu67 lie in the Switch II region and activity studies on the E66A and E67A mutant proteins illustrated that these residues do not play a critical role in nucleotide hydrolysis (Ash *et al.*, 2011). Therefore, their role in the GTPase cycle of NFeoB remains unclear.

In the current study, we present five structures of the mutant proteins described above in various nucleotide-bound states. This suite of structures not only supports the findings from the functional characterization of these mutant proteins, but also together confirm the presence of, and reveal the structural basis for, nucleotide-dependent rigid-body movement of the helical domain in *S. thermophilus* NFeoB.

2. Materials and methods

2.1. Protein purification and crystallization

Point mutations T35S, T35A, E66A and E67A in *S. thermophilus* NFeoB (residues 1–270; accession code Q5M586) were introduced as described previously (Ash *et al.*, 2011). These mutant proteins were expressed as N-terminally tagged GST-fusion proteins from a pGEX-4T-1 vector and purified *via* affinity and gel-filtration chromatography as described in Ash *et al.* (2011). Removal of the GST tag by thrombin cleavage left two additional amino acids, Gly-Ser, preceding the start methionine at the N-terminus of the protein. These two amino acids therefore remained in the final purified and crystallized constructs. Purified proteins were concentrated to approximately 10 mg ml^{-1} in buffer consisting of 20 m*M* Tris pH 8.0 and 100 m*M* NaCl using a spin concentrator (10 kDa molecular-weight cutoff; Millipore) and stored at 193 K in the same buffer until use in crystallization experiments. Protein concentrations were determined using the BCA assay method (Smith *et al.*, 1985).

All crystallization trials were performed at 293 K using the hanging-drop vapour-diffusion method with commercially available screens (PACT, JCSG+ and Classics Suites; Qiagen). Initial screening experiments were conducted in 96-well format using a Mosquito nanolitre liquid-handling robot (TTP LabTech), with drops containing equal volumes (150 nl) of reservoir and protein solution. All crystals were obtained through cocrystallization experiments with different nucleotides. GDP and mantGMPPNP (mGMPPNP; a fluorescently labelled nonhydrolyzable GTP analogue) were obtained from Invitrogen and GMPPNP (an unlabelled nonhydrolyzable GTP analogue) was obtained from Jena Bioscience. The compositions of each protein/nucleotide mixture and the final crystallization conditions for each structure are presented in

Table 2
Crystallographic data-processing and refinement statistics.

Values in parentheses are for the highest resolution shell.

	GDP^N–T35A	Apo-T35S	mGMPPNP–E67A	GDP–E67A	GMPPNP–E66A
Data processing					
Wavelength (Å)	0.95370	0.95370	0.95369	0.95369	0.95370
Space group	$P4_12_12$	$P2_12_12_1$	$C222_1$	$P2_12_12_1$	$P2_12_12_1$
Unit-cell parameters					
a (Å)	42.8	44.4	49.2	64.6	48.7
b (Å)	42.8	59.9	82.7	92.1	74.4
c (Å)	281.2	85.3	150.9	206.8	156.1
Resolution (Å)	50–2.50 (2.54–2.50)	50–2.65 (2.70–2.65)	50–1.85 (1.88–1.85)	50–2.50 (2.54–2.50)	50–2.60 (2.64–2.60)
Total reflections	101278	48223	107492	210888	104112
Unique reflections	9980 (431)	7047 (343)	26037 (1257)	43672 (2110)	17841 (787)
Completeness (%)	99.3 (89.2)	99.8 (98.6)	97.2 (96.3)	98.5 (98.3)	99.3 (89.4)
$\langle I/\sigma(I)\rangle$	25.1 (2.3)	16.3 (2.1)	15.3 (1.90)	16.6 (2.5)	11.5 (2.1)
⟨Multiplicity⟩	10.1 (3.4)	6.8 (4.9)	4.1 (4.1)	4.8 (4.5)	5.8 (4.5)
$R_{\rm merge}$†	0.079 (0.358)	0.119 (0.648)	0.072 (0.762)	0.085 (0.548)	0.153 (0.574)
Refinement					
No. of molecules per asymmetric unit	1	1	1	4	2
No. of atoms	2019	1921	2184	8130	4130
No. of water molecules	28	9	113	110	57
Resolution	42.3–2.50 (2.56–2.50)	49.0–2.65 (2.72–2.65)	41.4–1.85 (1.89–1.85)	50.0–2.50 (2.57–2.50)	46.5–2.61 (2.68–2.61)
Unique reflections	9797 (634)	6959 (489)	25910 (1702)	42786 (3105)	17682 (1161)
Completeness (%)	98.3 (90.1)	99.0 (97.0)	96.3 (87.3)	98.2 (98.2)	98.6 (89.0)
R.m.s.d. bonds (Å)	0.010	0.010	0.010	0.009	0.010
R.m.s.d. angles (°)	1.483	1.39	1.43	1.40	1.44
⟨Protein B factor⟩ (Å^2)	35.9	48.4	37.1	47.1	25.1
Ramachandran plot‡					
Favoured (%)	97.2	98.0	97.0	98.4	97.1
Allowed (%)	100	100	100	100	100
$R_{\rm work}$§	0.220	0.219	0.185	0.217	0.214
$R_{\rm free}$¶	0.260	0.284	0.223	0.259	0.259
PDB code	3b1y	3b1z	3b1v	3b1w	3b1x

† $R_{\rm merge} = \sum_{hkl}\sum_i |I_i(hkl) - \langle I(hkl)\rangle| / \sum_{hkl}\sum_i I_i(hkl)$. ‡ As calculated by *MolProbity* (Chen *et al.*, 2010) § $R_{\rm work} = \sum_{hkl} \big||F_{\rm obs}| - |F_{\rm calc}|\big| / \sum_{hkl} |F_{\rm obs}|$. ¶ Calculated as for $R_{\rm work}$ using 5% of the diffraction data which were excluded during refinement. For GDP^N–T35A and apo-T35S 10% of the diffraction data were excluded for the calculation of $R_{\rm free}$.

Table 1. Except for GDP–E67A, diffraction-quality crystals were obtained directly from initial screening trials without further optimization. Crystals of GDP–E67A were optimized in 24-well trays (Hampton Research) in hanging drops consisting of equal volumes (1 µl) of protein solution and reservoir solution equilibrated over 0.5 ml reservoir solution. Optimization involved varying the precipitant concentration and pH, which ultimately produced rod-shaped diffraction-quality crystals.

All crystals were flash-cooled in liquid nitrogen after brief immersion in the relevant cryoprotectant solution. Crystals of mGMPPNP–E67A, GMPPNP–E66A and GDP^N–T35A were cryoprotected in mother liquor with 20% glycerol, GDP–E67A was cryoprotected in a solution consisting of 50%(*w*/*v*) saturated sucrose prepared in mother liquor and apo-T35S was immersed in unmodified mother liquor before cooling.

2.2. Data collection and processing

Diffraction data for mGMPPNP–E67A and GDP–E67A were recorded on beamline MX2 at the Australian Synchrotron using an ADSC Quantum 315r detector. Data for all remaining crystals were recorded on beamline MX1 at the Australian Synchrotron using an ADSC Quantum 210r detector (McPhillips *et al.*, 2002). All data were processed and scaled using the *HKL*-2000 suite (Otwinowski & Minor, 1997).

2.3. Structure solution and refinement

The crystals of mGMPPNP–E67A and GDP^N–T35A were isomorphous with wild-type mGMPPNP-bound (PDB entry 3lx5; Ash *et al.*, 2010) and GDP-bound (PDB entry 3lx8; Ash *et al.*, 2010) $NFeoB^{St}$, respectively. After removal of all non-protein atoms, these wild-type structures were used as starting models for rigid-body refinement with the mutant data. All other mutant structures were solved by molecular replacement using the program *Phaser* (McCoy *et al.*, 2007) from the *CCP*4 program suite (Winn *et al.*, 2011). For GMPPNP–E66A, the model of wild-type $NFeoB^{St}$ bound to mGMPPNP was used as a search model after removal of all nonprotein atoms. The structure of wild-type $NFeoB^{St}$ bound to GDP was similarly modified before being used as a molecular-replacement model for GDP–E67A and apo-T35S. Structure refinements were carried out using *REFMAC* v.5.5.0109 (Murshudov *et al.*, 2011) with TLS (Winn *et al.*, 2001) and manual model building was performed in *Coot* (Emsley & Cowtan, 2004). An anomalous difference Fourier map for mGMPPNP–E67A was constructed using *Phaser*. All structure figures were generated using *MacPyMOL* (Schrödinger LLC). The sequences were aligned using *ClustalW*2 (Chenna *et al.*, 2003) and sequence-alignment figures were generated using the program *ALINE* (Bond & Schüttelkopf, 2009). Three-dimensional coordinate interpolations were performed using the corkscrew method

in the *UCSF Chimera* package (Resource for Biocomputing, Visualization and Informatics at the University of California, San Francisco).

3. Results

3.1. Crystallization of GDP^{N}–T35A and apo-T35S

As in other small G-proteins, Thr35 lies in the Switch I region and encompasses the fully conserved G2 motif (Supplementary Fig. 1[1]). The mutation of Thr35 to alanine or serine in *S. thermophilus* NFeoB abolished GTPase activity (Ash *et al.*, 2011), presumably owing to loss of Mg^{2+} coordination and disruption of the native GTP-bound Switch I structure. To explore the effect of T35A and T35S mutations on the structure of NFeoBSt, we attempted cocrystallization experiments in the presence of high concentrations of the nonhydrolyzable GTP analogue GMPPNP. Crystals of both mutant proteins were obtained and the data-processing and refinement statistics for these and other structures are presented in Table 2.

Upon inspection of the electron-density maps it became evident that neither crystal contained GMPPNP. Instead, the nucleotide-binding site was unoccupied in the crystals of T35S and unambiguously contained a diphosphate nucleotide in the crystals of T35A. The diphosphate nucleotide in the latter structure results from the slow but spontaneous hydrolysis of GMPPNP at pH 6.0 in the crystallization drop over the month that the crystals took to form. Although such nucleotides are considered to be 'nonhydrolyzable' on the time scale used for most nucleotide-binding experiments, spontaneous hydrolysis nonetheless occurs over weeks at ambient temperatures and particularly at pH < 7.0 (GMPPNP specification sheet, Jena Bioscience). The major non-enzymatic breakdown product of such nucleotides is the phosphoramidate XMPPN (where X is any base), in which a primary amine is substituted for one of the β-phosphate O atoms (Meyer *et al.*, 2003; Yount *et al.*, 1971). Therefore, we have modelled the diphosphate nucleotide in the structure of T35A as GMPPN (referred to as GDP^{N} in further discussion), a designation that has similarly been made by others after cocrystallization with XMPPNP nucleotides (Olesen *et al.*, 2007; Ferguson *et al.*, 2011). The interactions between the GDP^{N} nucleotide and the active site of T35A are unchanged relative to those observed in the GDP-bound form of the wild-type protein (Ash *et al.*, 2010).

3.2. Overall structures of GDP^{N}–T35A and apo-T35S

GDP^{N}–T35A and apo-T35S both share the same overall structure as wild-type NFeoBSt, in which residues 1–160 exhibit the canonical G-protein fold and residues 171–270 form an α-helical domain that packs against one side of the G-domain (Fig. 1). The interactions between the G-domain and the helical domain have been thoroughly described for *Thermotoga maritima* NFeoB (Hattori *et al.*, 2009). Residues 161–170 form a linker between the two domains.

The structures of the two Switch regions in GDP^{N}–T35A and apo-T35S are highlighted in Fig. 1. Switch I (residues 24–37) forms an additional β-strand against the β-sheet core of the protein and the Switch II helix (residues 61–77) lies at the interface between the G-domain and the helical domain. The conformations of both of these Switch regions overlay with those from the GDP-bound form of the wild-type protein rather than the GTP-bound form. The overall r.m.s. deviation between wild-type GDP-bound NFeoBSt and the two mutant structures is 0.4 and 0.7 Å over all common C$^{\alpha}$ atoms for T35A and T35S, respectively. These structures therefore illustrate that although mutation of Thr35 abolishes the GTPase activity

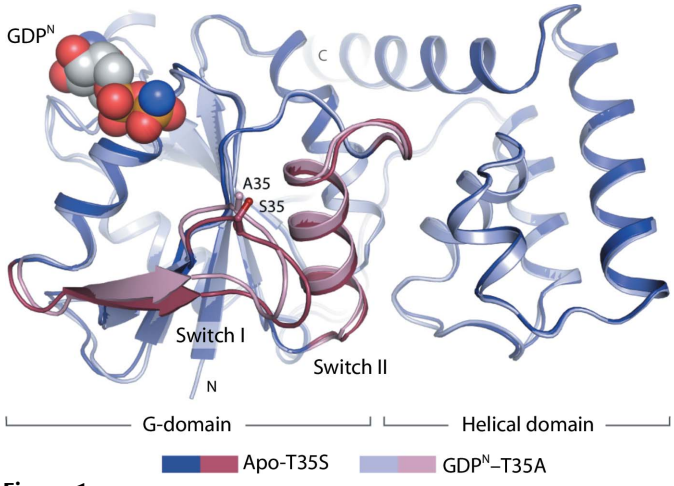

Figure 1
Structural overview of Thr35 mutant proteins. Superposition of apo-T35S (dark blue) and GDP^{N}–T35A (light blue). The Switch regions are coloured dark and light pink for apo-T35S and GDP^{N}–T35A, respectively. The mutant Ala35 and Ser35 side chains are shown as sticks and the GDP^{N} nucleotide is shown as spheres.

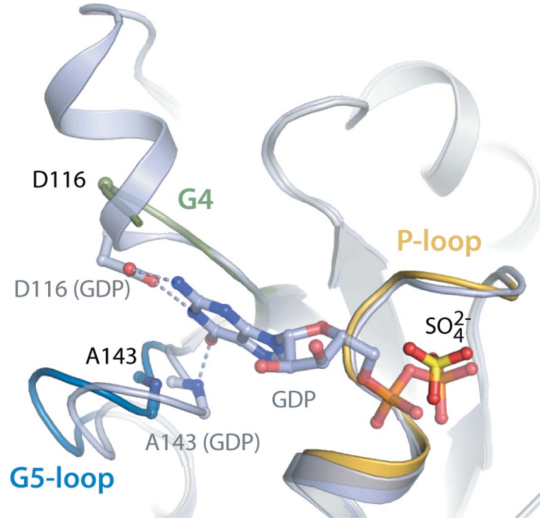

Figure 2
Structural changes at the active site in apo-T35S. Comparison between the active sites of apo-T35S and GDP-bound wild-type NFeoBSt (light blue). The P-loop from apo-T35S is coloured yellow, the G4 motif is coloured green and the G5 loop is coloured blue.

[1] Supplementary material has been deposited in the IUCr electronic archive (Reference: HV5199). Services for accessing this material are described at the back of the journal.

of NFeoBSt, the overall structural integrity of the mutant proteins in their apo and GDP-bound forms have not been compromised. Changes in GTP binding and GTPase activity in the T35A and T35S proteins therefore arise from disruption of the Mg^{2+}-binding site and hence the native GTP-bound Switch I structure.

3.3. Structural details of apo-T35S

At the active site in apo-T35S, a large 7σ peak of $F_o - F_c$ density was present in the position where the β-phosphate from GTP or GDP would sit. This peak could be perfectly described by modelling an SO_4^{2-} ion, which exhibits the same geometry as PO_4^{2-} and was present at 1 *M* concentration in the crystallization drop.

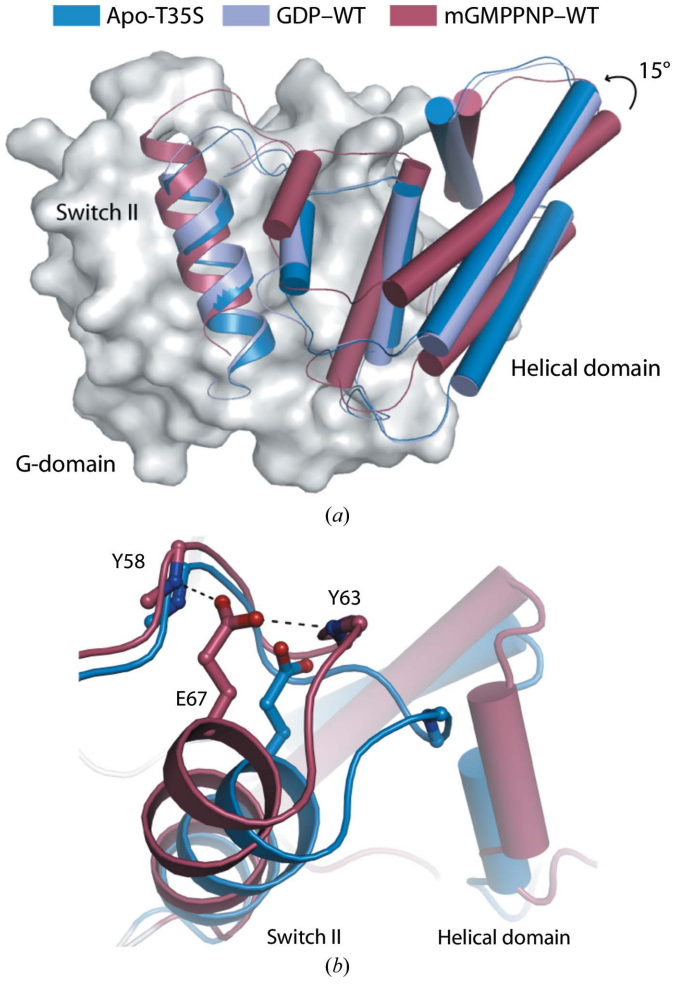

Figure 3
Nucleotide-dependent rigid-body movement in the helical domain. (*a*) Structural superposition of apo-T35S (blue), GDP–WT (light purple) and mGMPPNP–WT (pink). For the nucleotide-bound structures, coordinates were overlayed using substrate-directed superposition. This produced the best alignment of the G-domains of each protein and highlighted the movement of the helical domain relative to the G-domain. For apo-T35S, in which the nucleotide-binding site is unoccupied, superposition was performed against the G-domain of GDP–WT (r.m.s. deviation of 0.5 Å over 143 C^{α} atoms). Helices from the helical domain are shown as cylinders, while the Switch II helix is shown in traditional cartoon representation. The G-domain is shown as a surface. (*b*) Switch II loop conformation in apo-T35S (blue) and mGMPPNP–WT (pink). The Glu67 Switch II loop bridge is shown as dashed lines.

The structure of apo-T35S is the first time that *S. thermophilus* NFeoB has been visualized without nucleotide. Relative to the nucleotide-bound NFeoBSt structures, apo-T35S has undergone two primary conformational rearrangements at the active site (Fig. 2). Firstly, owing to the absence of a hydrogen bond between Ala143 and the GTP or GDP guanine base, the G5 loop (residues 143–148) is situated approximately 3 Å further from the nucleotide-binding site in apo-T35S. The G4 motif has changed conformation in a similar manner and the side chain of Asp116, which interacts with the guanine base in nucleotide-bound NFeoB, is disordered in apo-T35S. In addition, the adjacent residues 118–123 are disordered in apo-T35S, in contrast to their defined α-helical conformation in GDP-bound and GTP-bound wild-type NFeoBSt.

The side chain of the mutated Ser35 residue is disordered in apo-T35S and, like Thr35 in the wild-type GDP-bound protein, it does not make any contacts with the greater protein. We may therefore consider this structure to be representative of the apo structure of wild-type NFeoBSt. The crystallization of apo NFeoBSt is significant, as it finally allows the complete structural reconstruction of the GTPase cycle of NFeoB.

3.4. The GTPase cycle of NFeoBSt reveals nucleotide-dependent movement of the helical domain

The apo-T35S structure completes the complement of models required to fully define all key structural states in the GTPase cycle of an NFeoB protein. These models include apo-T35S (PDB entry 3b1z, this work), mGMPPNP–WT (PDB entry 3lx5; Ash *et al.*, 2010), GDP–AlF_4^-–WT (PDB entry 3ss8; Ash *et al.*, 2011) and GDP–WT (PDB entry 3lx8; Ash *et al.*, 2010). Importantly, of all GMPPNP-bound NFeoB structures determined to date, that from *S. thermophilus* is the only one to display an ordered Switch I conformation. Furthermore, *S. thermophilus* is the only organism from which NFeoB has been crystallized in complex with a transition-state analogue. Therefore, we can now use these structures to model all of the transitions associated with GTP binding, hydrolysis and GDP release in NFeoB proteins. To illustrate some of these transitions, we have constructed a movie that highlights the overall structural rearrangements associated with each step in the GTPase cycle (Supplementary Movie 1).

When viewed as a movie, a large nucleotide-dependent rigid-body rearrangement of the helical domain becomes strikingly apparent. Upon conversion of apo to mGMPPNP-bound NFeoBSt, the helical domain pivots approximately 15° relative to the G-domain or *vice versa* (Fig. 3*a* and Supplementary Movie 1). Furthermore, movement of the helical domain is clearly related to movement of the Switch II region, while the rest of the G-domain remains stationary. This suggests that the identity of the nucleotide at the active site is indeed communicated to the helical domain through the Switch II region, as predicted (Hattori *et al.*, 2009; Petermann *et al.*, 2010).

3.5. Glu67 maintains the integrity of Switch II in *S. thermophilus* NFeoB

Interestingly, Glu67, which is a conserved residue in Switch II, appears to be involved in mediating movement of the apex of the Switch II loop away from the helical domain upon GTP binding (Fig. 3*b*). In GTP-bound NFeoBSt the side chain of Glu67 hydrogen bonds to the backbone amide N atoms of Tyr58 and Tyr63 from Switch II, forming a 'Switch II bridge'. Yet when the protein is in the apo form or bound to GDP, the Switch II bridge is absent and Switch II adopts a relaxed conformation that projects towards the helical domain.

To determine the potential significance of this, two structures of E67A were determined: one bound to mGMPPNP and the other to GDP. mGMPPNP is a fluorescently labelled version of the nonhydrolyzable GTP analogue GMPPNP in which an *N*-methylanthraniloyl (mant) group is covalently attached to the ribose ring of the nucleotide. The mant group was fully disordered in mGMPPNP–E67A and did not form any contacts with the protein. Fig. 4(*a*) shows a superposition between mGMPPNP–E67A and GDP–E67A. Both structures agree well with the equivalent forms of the wild-type protein, having r.m.s. deviations of 0.5 and 0.8 Å over all common C$^{\alpha}$ atoms, respectively.

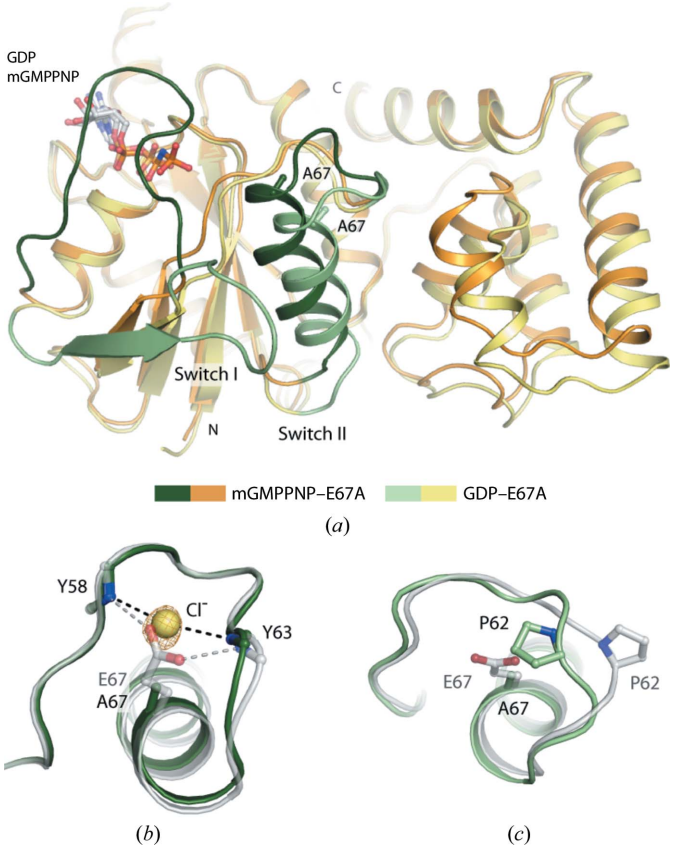

Figure 4
Structures of mGMPPNP–E67A and GDP–E67A. (*a*) Superposition of mGMPPNP–E67A (orange) and GDP–E67A (yellow). The Switch regions are coloured dark and light green for mGMPPNP–E67A and GDP–E67A, respectively. The nucleotide molecules and the Ala67 side chain are shown as sticks. The fully disordered mant group has been omitted from this and other figures for clarity. (*b*) Structure of the Switch II loop in mGMPPNP–E67A (dark green). The structure of wild-type mGMPPNP-bound NFeoBSt is overlayed as a transparent grey cartoon and sticks. An anomalous difference Fourier map for mGMPPNP–E67A contoured at 3σ is shown in orange. (*c*) Structure of the Switch II loop in chains *A* and *C* in GDP–E67A (light green). The structure of wild-type GDP-bound NFeoBSt is overlayed as a transparent grey cartoon and sticks.

Close examination of the structure of mGMPPNP–E67A illustrates the importance of Glu67 in maintaining the conformational details of Switch II in the GTP-bound form of the protein. In the initial rounds of refinement, a large sphere of positive $F_o - F_c$ electron density was apparent in place of the Glu67 side chain. The size of the peak suggested that it arose from a bound ion rather than a water molecule and the construction of a likelihood-based anomalous difference Fourier map indeed produced a 14σ peak in this position (Fig. 4*b*). The peak was 1.7 times larger than the anomalous difference peak on the nucleotide β-P atom, consistent with its arising from a chloride ion, which possesses a scattering factor 1.6 times larger than phosphorus at the data-collection energy. Therefore, the peak was modelled as a chloride ion, which (i) was present at 150 m*M* in the crystallization drop, (ii) matches the charge of the wild-type Glu67 side chain, (iii) satisfied the electron density upon refinement and (iv) produced a refined *B*-factor matching those of surrounding residues.

The chloride ion in mGMPPNP–E67A has structurally replaced the Glu67 side chain and, like Glu67 in the wild-type protein, the ion is the recipient of two hydrogen bonds from Tyr58 and Tyr63 (Fig. 4*b*). The structure therefore suggests that the GTP-bound Switch II conformation in NFeoBSt is accompanied by stabilizing ionic interactions arising either from Glu67 in the native protein or from the chloride ion in mGMPPNP–E67A.

The side chain of Glu67 also appears to play a minor role in maintaining the structural details of Switch II in the GDP-bound form of NFeoBSt. There are four molecules in the asymmetric unit of the crystals of GDP–E67A that do not differ in global conformation (the average r.m.s. deviation between all pairs of molecules is 0.6 Å over all C$^{\alpha}$ atoms). In chains *B* and *D* the Switch II loop possesses the same conformation as the wild-type protein. In chains *A* and *C*, however, the mutation of Glu67 has permitted local conformational change in the apex of Switch II in order to satisfy the crystal-packing requirements of these molecules. Here, the Switch II loop backbone at Pro62 has moved 4 Å relative to its position in the wild-type protein, a conformation that would cause a steric clash with the side chain of Glu67 in the wild-type protein (Fig. 4*c*). Therefore, the absence of Glu67 has increased the conformational freedom of the Switch II region in the GDP-bound form of the protein.

3.6. Glu66 does not influence the structure of Switch II

Glu66 is conserved in all FeoB proteins as either an aspartate or glutamate (Supplementary Fig. 1) and lies in the Switch II region. Despite its close proximity to the nucleotide γ-phosphate, mutation of Glu66 to alanine in NFeoBSt had no effect on nucleotide binding or hydrolysis. However, the

equivalent residue has been shown to be essential for *in vivo* iron transport in full-length *E. coli* FeoB (Eng *et al.*, 2008) and thus its structural and functional importance remained unclear. The structure of E66A bound to GMPPNP has been determined to 2.60 Å resolution. The overall structure of the protein is unaffected by the mutation (r.m.s. deviation of 0.6 Å over all C^{α} atoms relative to the wild-type mGMPPNP-bound protein) and there are no structural rearrangements in the Switch II region where the mutation is located. This structure therefore highlights the need for further studies to examine the role of Glu66 in the context of the full-length protein.

4. Discussion

The current suite of structures complements the results from earlier functional characterization of the *S. thermophilus* NFeoB mutant proteins (Ash *et al.*, 2011), confirming their overall structural integrity and revealing the details of how they interact with nucleotides. Furthermore, evidence has been presented for nucleotide-dependent helical domain movement in $NFeoB^{St}$, a feature that has been predicted (Hattori *et al.*, 2009; Petermann *et al.*, 2010) but for which no structural confirmation has yet been available, despite the plethora of structural data on NFeoB proteins. Other reported GMPPNP-bound NFeoB structures differed little from those of their GDP-bound counterparts, since either or both of the Switch I and Switch II loops remained in their GDP-bound conformations.

Based on inspection of the active sites in apo and mGMPPNP-bound $NFeoB^{St}$ and also the Glu67 mutant structures, we propose a mechanism by which structural changes at the nucleotide-binding site are communicated to the helical domain *via* rearrangements in Switch II (Fig. 5). The catalyst for all downstream structural rearrangements is the reorientation of the G3 motif and Switch I upon MgGTP binding. In the GTP-bound form of the protein the G3 motif (^{53}DLPG^{56}) interacts with the nucleotide γ-phosphate and one of the magnesium-coordinated water molecules. For these interactions to take place, the backbone of the G3 motif moves almost 3 Å away from Switch II (Fig. 5*a*). MgGTP binding also causes Switch I reorientation, displacing two bulky hydrophobic side chains (Trp31 and Val36) from a cavity adjacent to Switch II, such that Switch II tilts towards the greater G-domain (Figs. 5*a* and 5*b*). In addition, Switch II shifts vertically (as drawn) to preserve the tight packing of the hydrophobic core of the protein through the side chain of Tyr73. These movements in Switch II promote the concerted rigid-body movement of the tightly packed helical domain in the same direction (Fig. 5*a*). The Switch II bridge formed by Glu67 appears to be important for permitting this structural rearrangement by shifting the Switch II loop apex away from the helical domain by ∼7.0 Å (Fig. 5*a*). Other species-specific interactions between the helical domain and the Switch II

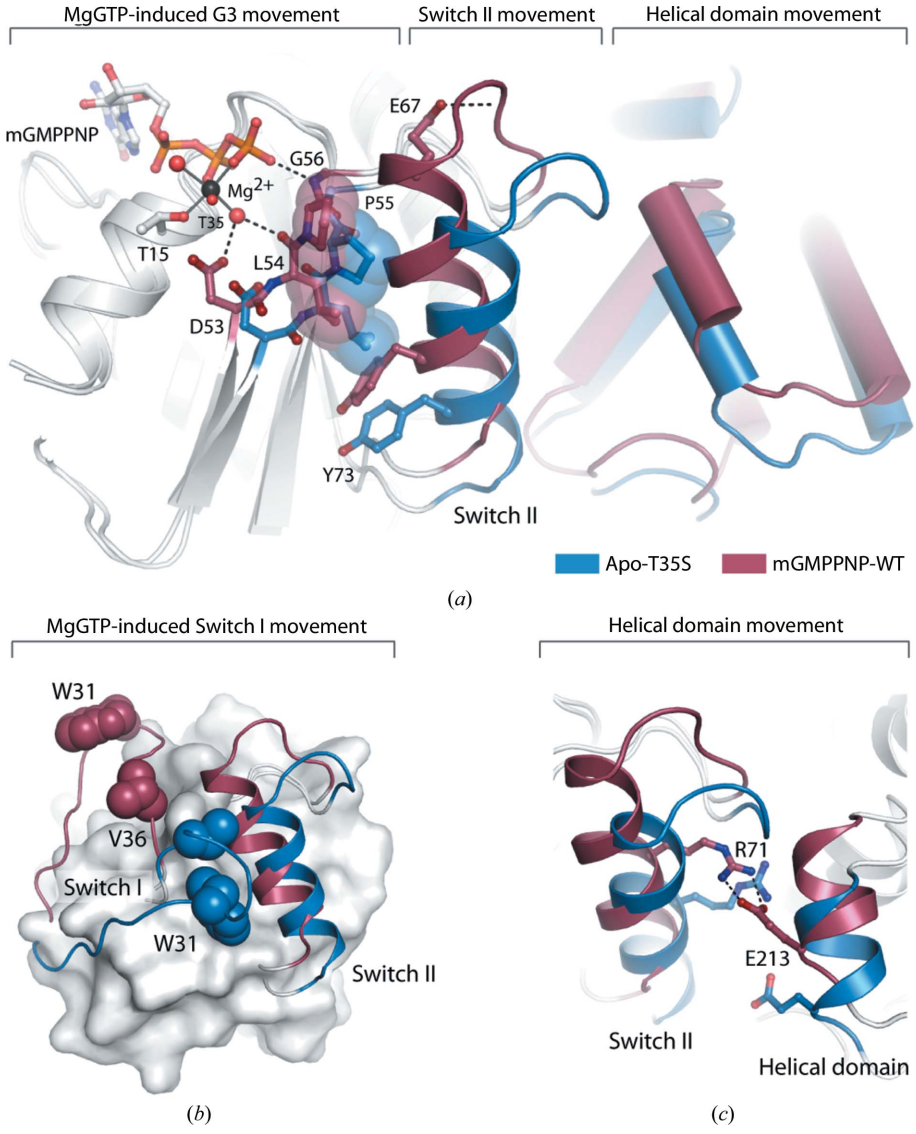

Figure 5
Structural basis for GTP-induced helical domain movement in $NFeoB^{St}$. (*a*) Structural superposition of apo-T35S (blue) and mGMPPNP–WT (pink), with important regions for helical domain movement shown in colour. Switch I has been omitted from the figure for clarity and nucleotide-dependent changes in the Switch I conformation are instead represented in (*b*). In omitting Switch I from the figure, the side-chain hydroxyl of Thr35 is shown as a small sphere. The helical domain is shown as a cylindrical cartoon. (*b*) GTP-induced changes in the conformation of Switch I. The helical domain has been omitted from the figure. Trp31 and Val36 are shown as spheres and the G-domain as a surface. (*c*) Salt bridge between Arg71 from Switch II and Glu213 from the helical domain in the GTP-bound form of the protein.

region could also be important in the structural communication between the two domains (such as between Arg71 and Glu213 in *S. thermophilus* NFeoB; Fig. 5*c*); however, these must be addressed on a case-by-case basis owing to the poor sequence conservation of the helical domain across different prokaryotic species. When GTP is hydrolyzed to GDP, the G3 motif and Switch I relax back to their resting conformations and return the helical domain to its apo orientation (Fig. 3*a*). Central to this structural reversion is not only loss of the γ-phosphate, but also dissociation of magnesium from the active site in GDP-bound NFeoB. None of the deposited GDP-bound NFeoB structures have contained a magnesium ion at the active site (Guilfoyle *et al.*, 2009; Hattori *et al.*, 2009; Köster *et al.*, 2009; Ash *et al.*, 2010; Hung *et al.*, 2010) and it thus appears that the ion is not retained in the GDP-bound form of the protein. This ensures full relaxation of the G3 motif after nucleotide hydrolysis and the concomitant movement of Switch II.

The observed Switch II-mediated helical domain movement in *S. thermophilus* NFeoB is typical for a multi-domain G-protein (Wittinghofer & Vetter, 2011). The Switch regions in such G-proteins are often located at domain interfaces with the explicit purpose of inducing functionally significant nucleotide-dependent domain rearrangements (Wittinghofer & Vetter, 2011). In FeoB, the helical domain is present in all FeoB proteins without any exception known to us and the integrity of the interface between the G-domain and the helical domain is essential for iron uptake (Eng *et al.*, 2008; Hattori *et al.*, 2009). The current suite of structures has opened up the possibility that GTPase-induced helical domain movement could be communicated to the C-terminal iron-uptake domain, to which it is directly tethered. The structural determination of full-length FeoB is now required in order to determine whether the domain rearrangements observed in *S. thermophilus* NFeoB do indeed play a role in transmembrane gating in this unique G-protein-coupled iron transporter.

This study was supported by the National Health and Medical Research Council (grant Nos. 570784 and 632703). This research was undertaken on the MX1 and MX2 beamlines at the Australian Synchrotron, Victoria, Australia. MJM is a Cancer Institute of NSW Career Development Fellow. M-RA is the recipient of an Australian Postgraduate Award.

References

Ash, M.-R., Guilfoyle, A., Clarke, R. J., Guss, J. M., Maher, M. J. & Jormakka, M. (2010). *J. Biol. Chem.* **285**, 14594–14602.
Ash, M.-R., Maher, M. J., Guss, J. M. & Jormakka, M. (2011). *PLoS One*, **6**, e23355.
Bond, C. S. & Schüttelkopf, A. W. (2009). *Acta Cryst.* D**65**, 510–512.
Chen, V. B., Arendall, W. B., Headd, J. J., Keedy, D. A., Immormino, R. M., Kapral, G. J., Murray, L. W., Richardson, J. S. & Richardson, D. C. (2010). *Acta Cryst.* D**66**, 12–21.
Chenna, R., Sugawara, H., Koike, T., Lopez, R., Gibson, T. J., Higgins, D. G. & Thompson, J. D. (2003). *Nucleic Acids Res.* **31**, 3497–3500.
Dashper, S. G., Butler, C. A., Lissel, J. P., Paolini, R. A., Hoffmann, B., Veith, P. D., O'Brien-Simpson, N. M., Snelgrove, S. L., Tsiros, J. T. & Reynolds, E. C. (2005). *J. Biol. Chem.* **280**, 28095–28102.
Emsley, P. & Cowtan, K. (2004). *Acta Cryst.* D**60**, 2126–2132.
Eng, E. T., Jalilian, A. R., Spasov, K. A. & Unger, V. M. (2008). *J. Mol. Biol.* **375**, 1086–1097.
Ferguson, A. D., Sheth, P. R., Basso, A. D., Paliwal, S., Gray, K., Fischmann, T. O. & Le, H. V. (2011). *FEBS Lett.* **585**, 104–110.
Guilfoyle, A., Maher, M. J., Rapp, M., Clarke, R., Harrop, S. & Jormakka, M. (2009). *EMBO J.* **28**, 2677–2685.
Hantke, K. (2003). *Trends Microbiol.* **11**, 192–195.
Hattori, M., Jin, Y., Nishimasu, H., Tanaka, Y., Mochizuki, M., Uchiumi, T., Ishitani, R., Ito, K. & Nureki, O. (2009). *Structure*, **17**, 1345–1355.
He, J., Miyazaki, H., Anaya, C., Yu, F., Yeudall, W. A. & Lewis, J. P. (2006). *Infect. Immun.* **74**, 4214–4223.
Hung, K.-W., Chang, Y.-W., Eng, E. T., Chen, J.-H., Chen, Y.-C., Sun, Y.-J., Hsiao, C.-D., Dong, G., Spasov, K. A., Unger, V. M. & Huang, T. (2010). *J. Struct. Biol.* **170**, 501–512.
Köster, S., Wehner, M., Herrmann, C., Kühlbrandt, W. & Yildiz, O. (2009). *J. Mol. Biol.* **392**, 405–419.
Marlovits, T. C., Haase, W., Herrmann, C., Aller, S. G. & Unger, V. M. (2002). *Proc. Natl Acad. Sci. USA*, **99**, 16243–16248.
McCoy, A. J., Grosse-Kunstleve, R. W., Adams, P. D., Winn, M. D., Storoni, L. C. & Read, R. J. (2007). *J. Appl. Cryst.* **40**, 658–674.
McPhillips, T. M., McPhillips, S. E., Chiu, H.-J., Cohen, A. E., Deacon, A. M., Ellis, P. J., Garman, E., Gonzalez, A., Sauter, N. K., Phizackerley, R. P., Soltis, S. M. & Kuhn, P. (2002). *J. Synchrotron Rad.* **9**, 401–406.
Meyer, A. S., Gillespie, J. R., Walther, D., Millet, I. S., Doniach, S. & Frydman, J. (2003). *Cell*, **113**, 369–381.
Murshudov, G. N., Skubák, P., Lebedev, A. A., Pannu, N. S., Steiner, R. A., Nicholls, R. A., Winn, M. D., Long, F. & Vagin, A. A. (2011). *Acta Cryst.* D**67**, 355–367.
Naikare, H., Palyada, K., Panciera, R., Marlow, D. & Stintzi, A. (2006). *Infect. Immun.* **74**, 5433–5444.
Olesen, C., Picard, M., Winther, A. M., Gyrup, C., Morth, J. P., Oxvig, C., Møller, J. V. & Nissen, P. (2007). *Nature (London)*, **450**, 1036–1042.
Otwinowski, Z. & Minor, W. (1997). *Methods Enzymol.* **276**, 307–326.
Palmgren, M. G. & Nissen, P. (2011). *Annu. Rev. Biophys.* **40**, 243–266.
Petermann, N., Hansen, G., Schmidt, C. L. & Hilgenfeld, R. (2010). *FEBS Lett.* **584**, 733–738.
Rees, D. C., Johnson, E. & Lewinson, O. (2009). *Nature Rev. Mol. Cell Biol.* **10**, 218–227.
Robey, M. & Cianciotto, N. P. (2002). *Infect. Immun.* **70**, 5659–5669.
Smith, P. K., Krohn, R. I., Hermanson, G. T., Mallia, A. K., Gartner, F. H., Provenzano, M. D., Fujimoto, E. K., Goeke, N. M., Olson, B. J. & Klenk, D. C. (1985). *Anal. Biochem.* **150**, 76–85.
Velayudhan, J., Hughes, N. J., McColm, A. A., Bagshaw, J., Clayton, C. L., Andrews, S. C. & Kelly, D. J. (2000). *Mol. Microbiol.* **37**, 274–286.
Winn, M. D. *et al.* (2011). *Acta Cryst.* D**67**, 235–242.
Winn, M. D., Isupov, M. N. & Murshudov, G. N. (2001). *Acta Cryst.* D**57**, 122–133.
Wittinghofer, A. & Vetter, I. R. (2011). *Annu. Rev. Biochem.* **80**, 943–971.
Yount, R. G., Babcock, D., Ballantyne, W. & Ojala, D. (1971). *Biochemistry*, **10**, 2484–2489.